ACCOUNTS of chemical research

Article

pubs.acs.org/accounts

Ballistic Energy Transport in Oligomers

Natalia I. Rubtsova, Layla N. Qasim, Arkady A. Kurnosov, Alexander L. Burin, and Igor V. Rubtsov*

Department of Chemistry, Tulane University, New Orleans, Louisiana 70118, United States

Supporting Information

CONSPECTUS: The development of nanocomposite materials with desired heat management properties, including nanowires, layered semiconductor structures, and self-assembled monolayer (SAM) junctions, attracts broad interest. Such materials often involve polymeric/oligomeric components and can feature high or low thermal conductivity, depending on their design. For example, in SAM junctions made of alkane chains sandwiched between metal layers, the thermal conductivity can be very low, whereas the fibers of ordered polyethylene chains feature high thermal conductivity, exceeding that of many pure metals. The thermal conductivity of nanostructured materials is determined by the energy transport between and within each component of the material, which all need to be understood for optimizing the properties. For example, in the SAM junctions, the energy transport across the metal-chain interface as well as the transport through the chains both determine the overall heat conductivity, however, to separate these contributions is difficult.

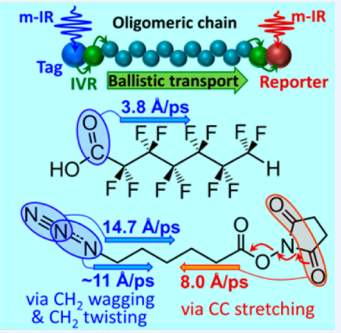

Recently developed relaxation-assisted two-dimensional infrared (RA 2DIR) spectroscopy is capable of studying energy transport in individual molecules in the time domain. The transport in a molecule is initiated by exciting an IR-active group (a tag); the method records the influence of the excess energy on another mode in the molecule (a reporter). The energy transport time can be measured for different reporters, and the transport speed through the molecule is evaluated. Various molecules were interrogated by RA 2DIR: in molecules without repeating units (disordered), the transport mechanism was expected and found to be diffusive. The transport via an oligomer backbone can potentially be ballistic, as the chain offers delocalized vibrational states. Indeed, the transport regime via three tested types of oligomers, alkanes, polyethyleneglycols, and perfluoroalkanes was found to be ballistic, whereas the transport within the end groups was diffusive. Interestingly, the transport speeds via these chains were different. Moreover, the transport speed was found to be dependent on the vibrational mode initiating the transport. For the difference in the transport speeds to be explained, the chain bands involved in the wavepacket formation were analyzed, and specific optical bands of the chain were identified as the energy transporters. For example, the transport initiated in alkanes by the stretching mode of the azido end group (2100 cm^{-1}) occurs predominantly via the CH_2 twisting and wagging chain bands, but the transport initiated by the C=O stretching modes of the carboxylic acid or succinimide ester end groups occurs via C−C stretching and CH_2 rocking bands of the alkane chain. Direct formation of the wavepacket within the CH_2 twisting and wagging chain bands occurs when the transport is initiated by the N═N stretching mode (1270 cm-1) of the azido end-group. The transport via optical chain bands in oligomers involves rather large vibrational quanta (700−1400 cm^{-1}), resulting in efficient energy delivery to substantial distances. Achieved quantitative description of various energy transport steps in oligomers, including the specific contributions of different chain bands, can result in a better understanding of the transport steps in nanocomposite materials, including SAM junctions, and lead towards designing systems for molecular electronics with a controllable energy transport speed.

1. INTRODUCTION

The development of new materials with unique energy transport landscapes has attracted broad interest. Nanomaterials, such as nanowires,[1,2] layered semiconductor structures,[3] and nanocomposites[4,5] featuring small thermal conductivity, have been designed. Nanocomposites of oligomeric components, such as self-assembled monolayer (SAM) junctions,[6] can have low[4] or high[7] thermal conductivity depending on the device architecture. Similarly, the thermal conductivity of ordered polyethylene fibers exceeds that of many pure metals,[8,9] whereas disordered polyethylene is a poor thermal conductor. Because of their low density, oligomeric materials are attractive candidates for energy dissipation in molecular electronics devices.[10] Nanostructured materials often consist of several components, and the energy transport within each component and between them has to be understood. For example, in SAM junctions with alkane chains sandwiched between metal layers, both the energy transport across the metal-chain interface and through the chain determine the overall heat conductivity;[11−13] however, it is difficult to separate these contributions, which limits the understanding of the overall energy transport process.

Several methods were recently developed for studying energy transport and thermal conductivity in mesoscopic materials, including 3ω modulation and time-domain thermoreflectance methods.[14−16] A temperature gradient is introduced with either a resistive heater or laser pulse. Energy distribution profiles are

Received: June 17, 2015
Published: August 25, 2015

DOI: 10.1021/acs.accounts.5b00299
Acc. Chem. Res. 2015, 48, 2547−2555

measured as a function of some parameters in the system linked to the sample size. A switch from the diffusive to ballistic mechanisms occurs with a decrease of sample thickness and is recorded experimentally by a change in the thermal conductivity coefficient.[14−16] In such measurements, requiring two dimensions to be macroscopic, the system temperature was typically near room temperature, resulting in the transport being governed by acoustic phonons.

Dlott and co-workers used a sum-frequency generation method to study energy transport in self-assembled monolayers of variable-length alkanes attached to a gold surface in response to laser-flash heating of the gold at ∼800 K and found that the through-chain transport is ballistic with a speed of 9.5 Å/ps.[12] It was suggested that optical chain bands are involved in the transport.[17] A ballistic contribution to energy transport was reported for single-wall carbon nanotubes,[2] alkane-bridged azulene-anthracene compounds,[18] and helices.[19]

The transport mechanism type, ballistic or diffusive, depends on the degree of delocalization of the states involved in the transport. Energy transport occurs ballistically when a wave-packet, coherent superposition of chain states delocalized over the transport distance, is excited and the coherence is preserved during the transport. Diffusive transport via Brownian-like hopping over localized vibrational states occurs otherwise.

2. THE RA 2DIR APPROACH PERMITS THE MEASUREMENT OF ENERGY TRANSPORT IN MOLECULES

Relaxation-assisted two-dimensional infrared (RA 2DIR) spectroscopy,[20−23] extending previously developed 2DIR spectroscopy,[24,25] permits measuring energy transport on a molecular scale in the time domain. The RA 2DIR method relies on the energy transport from an initially excited vibrational mode (tag) to the site where a probed mode (reporter) is located (Figure 1). When the excess energy arrives at the reporter site, the low frequency modes (ω_X), some of which are coupled strongly to the reporter (ω_2), become excited (Figure 1A). Probing the reporter by the probe mid-IR beam at corresponding delays involves the transitions to the combination state of modes 2 and X (Figure 1A) that feature a large anharmonicity, Δ_{X2}, and result in an increase of the tag-reporter, (ω_1, ω_2), cross peak amplitude (Figure 1D). The waiting time (delay between excitation of the tag (ω_1) and probing the reporter (ω_2)) at which the maximum cross peak amplitude is observed, T_{max}, is referred to as the energy transport time (Figure 1C). After reaching T_{max}, the cross peak decays due to further thermalization within the molecule and cooling to the solvent and levels to a plateau (Figure 1C) caused by the overall temperature increase in the sample (∼0.1 K or less) originating from the tag excitation.[26] Note that under small coupling conditions (Δ_{12} and $\Delta_{X2} \ll \sigma_2$), the cross-peak amplitude is proportional to the anharmonicity, whereas the cross-peak shape is governed by the spectral width (σ_2) of the transition.[23]

The highest sensitivity of the measurements can be achieved using dual-frequency three-pulse 2DIR spectroscopy with heterodyned detection (Figure 1E).[27] A fully automated instrument used for this research features the sensitivity of better than 10^{-4} cm^{-1} in measured anharmonicities, achieved by implementing closed-loop phase stabilization, phase cycling, beam-direction stabilization, spectral interferometry, and compact design.[28]

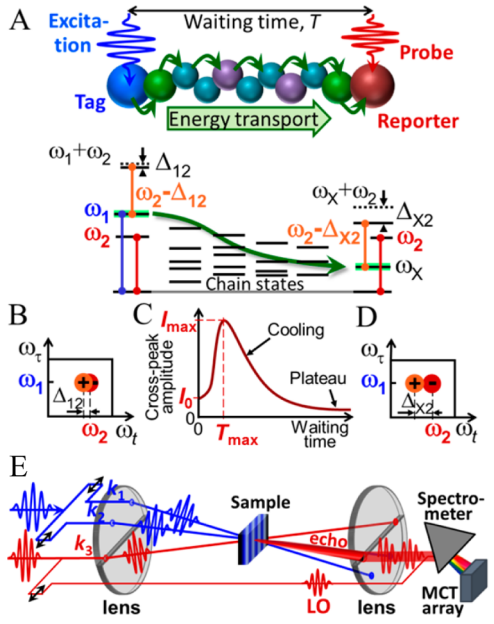

Figure 1. Principles of the RA 2DIR approach. (A) Energy diagrams show the tag (blue) and reporter (red/orange) transitions at small (left) and large (right) waiting times. 2DIR spectra at small (B) and large (D) waiting times. (C) Waiting-time dependence of the ω_1/ω_2 cross-peak amplitude. (E) Schematics of the dual-frequency three-pulse 2DIR instrument with heterodyned detection.

3. DIFFUSIVE ENERGY TRANSPORT

Earlier, RA 2DIR experiments were focused on energy transport in compounds ranging from organic molecules and peptides to transition metal complexes (for reviews, see refs 21 and 23). A correlation of the energy transport time with the tag-reporter distance found for numerous molecular systems lead to deciphering connectivity patterns in molecules using RA 2DIR.[22,29] In addition, the dependence of the energy transport time on molecular structure was reported.[30] The molecular backbones connecting the tags and reporters in these molecules contained bonds of different types and mode frequencies, which prevented delocalization of the high-frequency vibrational modes over extended backbone distances. The measured energy transport times were smaller than 10 ps, unless strongly affected by the long lifetime of the excited tag.[22,23] The energy transport under such conditions occurs via intramolecular vibrational energy redistribution (IVR) steps driven by anharmonic interactions of the involved modes.[31,32] The Fermi Golden Rule is often used to evaluate the rates of the vibrational relaxation processes,[33,34] although a way of introducing the width for all involved transitions needs to be specified. A novel theoretical approach for computing vibrational relaxation rates was recently developed that relies on using thermally populated low-frequency modes of the molecule itself as a bath providing fluctuations needed to make anharmonic transitions.[30,31] Such an approach predicts well the mode lifetimes and transport rates in systems interacting weakly with the solvent.[31,32]

Interestingly, even when the energy transport is governed by the random-walk IVR steps (often referred to as diffusive transport), the correlation of the energy transport time (T_{max}, Figure 1C) with the transport distance can be well-approximated as linear, albeit over a small range of distances (∼5 Å).[22,23,30] For example, such correlations are shown for the

DOI: 10.1021/acs.accounts.5b00299
Acc. Chem. Res. 2015, 48, 2547−2555

PBN (Figure 2) and CH3-s (Figure 3) compounds, where the transport to various reporters was initiated by the C≡N and

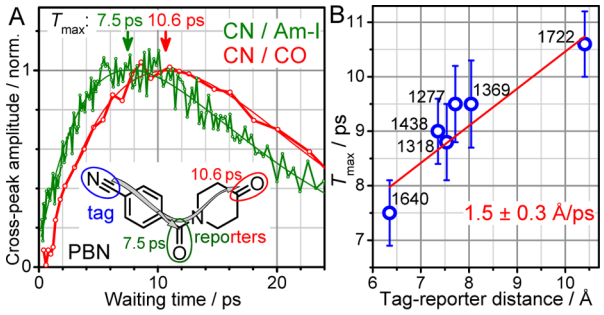

Figure 2. (A) Magnitude waiting-time traces for the indicated cross peaks for PBN (inset). (B) Dependence of T_{max} vs through-bond tag-reporter distance for cross peaks of PBN involving the ν(C≡N) tag and various reporters indicated by their frequencies in wavenumbers. The linear fit results in an effective speed of 1/slope = 1.5 ± 0.3 Å/ps (150 m/s).

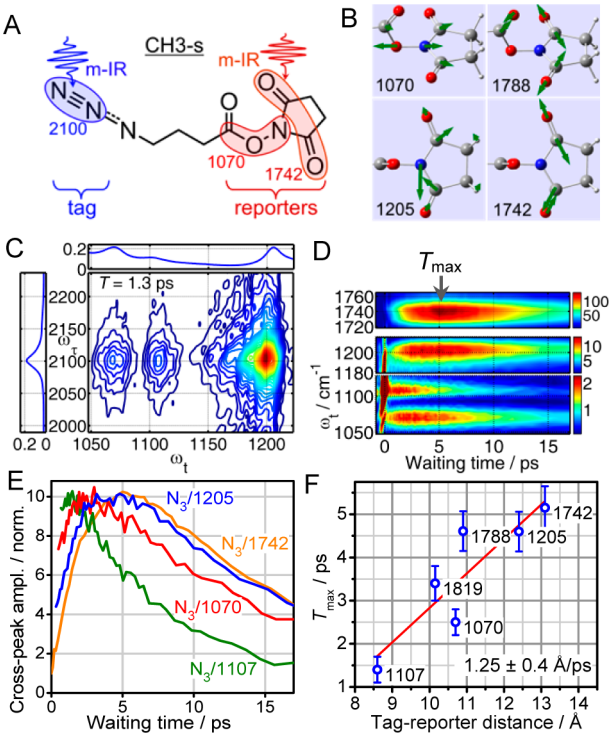

Figure 3. Diffusive energy transport in CH3-s. (A) Structure of CH3-s. (B) Normal mode displacements for indicated modes. (C) 2DIR magnitude spectrum of CH3-s in $CDCl_3$. (D) Absolute-value waiting-time dependences for cross peaks between the ν(N≡N) tag and several reporters. (E) Normalized waiting-time traces for the indicated cross peaks. (F) Dependence of T_{max} vs through-bond tag-reporter distance; frequencies of the reporters are indicated in wavenumbers.

N≡N stretching modes, respectively. The effective transport speeds calculated from the slope of the T_{max} relative to distance dependence (Figures 2B and 3F) were found to be similar: 1.5 ± 0.3 and 1.25 ± 0.4 Å/ps for PBN[23] and CH3-s,[35] respectively. Note that all T_{max} values for PBN are larger than those for CH3-s due to a long lifetime of the ν(C≡N) tag of 6.3 ps[22] compared to 1.1 ps for ν(N≡N) of CH3-s.[36]

The constant speed regime for a diffusive process is expected in the case of large losses from the molecule to the solvent.[32] Under such conditions, only the forward-directed IVR steps would result in the energy arrival to the reporter site with the overall transport time proportional to the minimum number of steps required, which in turn is proportional to the distance. The diffusive nature of the transport in CH3-s and PBN is concluded based on the localized character of their vibrational states[23] and small effective transport speeds compared to the transport in oligomers.[36,37]

4. BALLISTIC TRANSPORT VIA OLIGOMER CHAINS

The transport via an oligomeric chain can be ballistic if there are chain states delocalized over the region of the transport and a superposition (wavepacket) of these states is excited. The first RA 2DIR experiments performed with end-labeled PEG oligomers (Figure 4A) demonstrated that the transport occurs with a constant speed and can be observed over long distances of >60 Å.[36,37] Figure 4B shows the linear absorption spectrum of azPEG4 and motions of the reporter's modes; note that mode-C is also referred to as ν_{as}(C═O). Waiting time dependences for the cross peaks ν(N≡N)/mode-A in $CDCl_3$ and ν(N≡N)/mode-C in CCl_4 are shown in Figure 4C and D, respectively. The transport speeds (~5.5 Å/ps in $CDCl_3$ and ~5.1 Å/ps in CCl_4) are found to be much larger than those for the diffusive IVR transport, suggesting that the transport is ballistic (Figure 4G). A partially coiled structure is expected for PEG oligomers in solution[38] with mean end-to-end distances of 9.0 and 14.7 Å for azPEG4 and azPEG12 in chloroform, respectively.[36] Although these distances are much smaller than the through-bond distances, the through-bond transport is found to be dominant is these systems, as supported by several pieces of evidence. One piece of evidence is that the distance dependence of the cross-peak amplitude is not in agreement with the diffusive through-solvent transport (Figure 4H). In addition, a reporter with negligible temperature sensitivity (the mode-C frequency is ~20-fold less sensitive to temperature than that for mode-A)[26] is not expected to respond to temperature changes as the through-solvent transport occurs under quasi-equilibrium conditions. However, similar waiting time dependences were observed when mode-C was used as a reporter (Figure 4C and D). Although the chain coiling certainly could affect delocalization of the chain states, calculations suggest that even for coiled chains the states of PEG oligomers are largely delocalized (Figure 4E).[36] The coiling might change the transport efficiency (losses to the solvent), but the effect is not well studied.

Perfluoroalkanes are known to accept an extended, rodlike conformation in solution.[39] End-labeled perfluoroalkanes (CF*n*) featuring a carboxylic acid end-group serving as a tag and a CF_2H terminal group, where the C−H bending mode, δ(CH), at 1405 cm^{-1} served as a reporter (Figure 5), were studied. A constant-speed transport is found in CF*n* with a speed of 3.9 ± 0.4 Å/ps (Figure 5D).[39] This speed is somewhat slower than that for PEG chains but still much faster than the effective speed found for the diffusive transport regime, suggesting ballistic transport. Temperature dependent studies using CF5, CF7, and CF9 showed that the energy transport slows at higher temperatures (Figure 5E). A switch from the ballistic regime at lower temperatures to the diffusive regime at higher temperatures is suggested and supported by theoretical modeling.[40]

Recently, energy transport was studied in a series of end-labeled alkanes featuring an azido moiety at one end of the chain and succinimide ester (CH*n*-s) or carboxylic acid (CH*n*-

DOI: 10.1021/acs.accounts.5b00299
Acc. Chem. Res. 2015, 48, 2547−2555

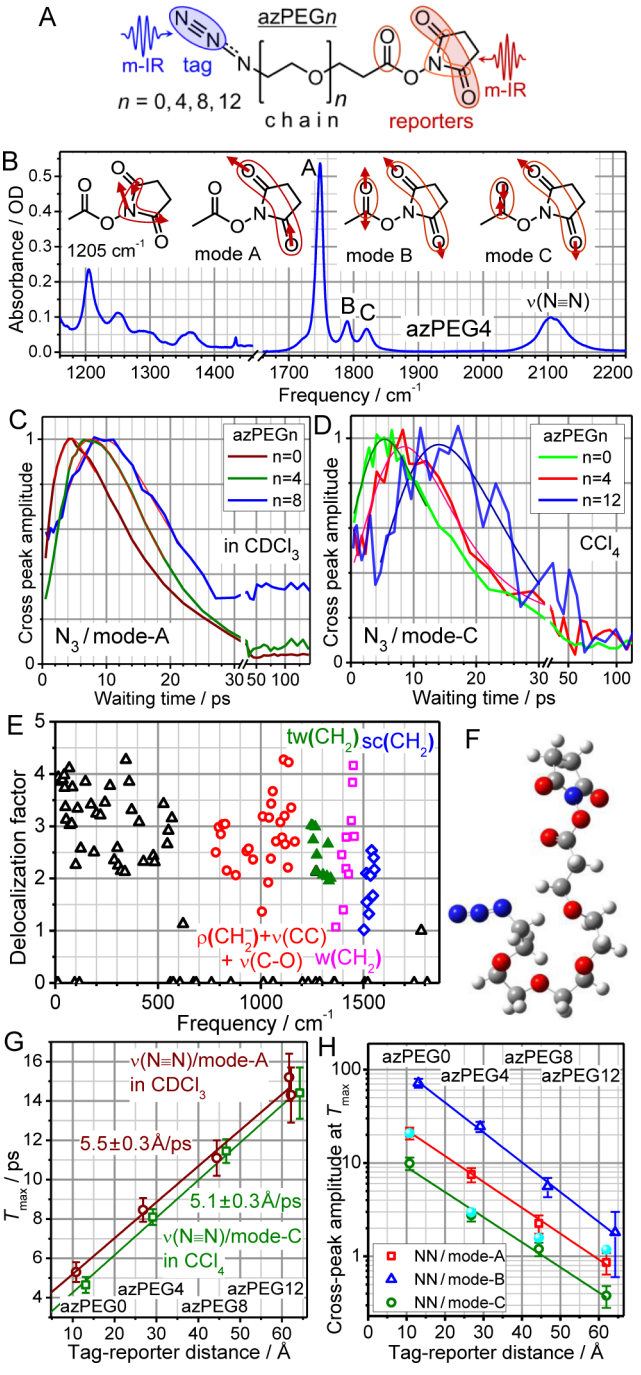

Figure 4. Ballistic energy transport through PEG chains. (A) Structure of azPEG*n*. (B) Linear absorption spectrum of azPEG4 in CCl_4; several characteristic normal modes are shown as insets. (C–D) Normalized waiting-time dependences for the indicated cross peaks. (E) Delocalization factor computed for all modes of azPEG4 adopting a coiled conformation shown in panel (F). (G) T_{max} vs distance dependence for indicated cross peaks. (H) Cross peak amplitude evaluated at T_{max} for the three cross peaks indicated vs tag-reporter distance. The best fits with a function, $y(L) = y_0 \exp(-L/L_0)$, result in L_0 of 13.6 ± 0.7, 15.6 ± 0.7, and 16.2 ± 1.6 Å for the cross peaks involving mode-A, mode-B, and mode-C reporters, respectively. Prediction for purely through-solvent energy transport is shown with cyan spheres.

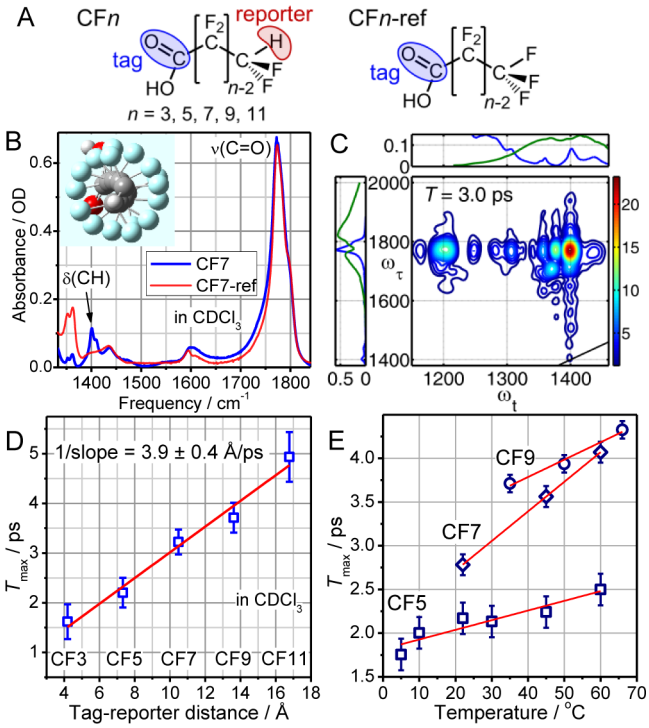

Figure 5. Ballistic energy transport via perfluoroalkane chains. (A) Structures of CF*n* and CF*n*-ref compounds. (B) Linear absorption spectra of CF7 and CF7-ref. (C) 2DIR spectrum of CF5. The linear absorption spectrum (blue) and the spectrum of the IR pulses (green) are shown in the attached panel. (D) T_{max} dependence of the tag-reporter distance. (E) Temperature dependence of T_{max} measured for CFn. A linear fit (red) resulted in the slopes of 0.011 ± 0.002, 0.034 ± 0.002, and 0.020 ± 0.003 ps/K for CF5, CF7, and CF9, respectively.

a) at the other end (Figure 6A). For the CH*n*-a compounds, the transport, initiated by the ν(N≡N) tag and recorded by the ν(C═O) reporter, was found to be the fastest among the oligomers (Figure 6B) with a speed of 14.4 ± 2 Å/ps (Figure 6D, open circles).[35] A similar speed of 14.7 ± 4 Å/ps was found in the CH*n*-s compounds when initiated by the ν(N≡N) tag and recorded by ν_{as}(C═O) of succinimide (Figure 6D, open stars). In addition, the energy transport dynamics was studied in the same compounds but with the tags and reporters switched (Figure 6A and C). Interestingly, the transport speed is slower when initiated by the carbonyl stretching modes compared to the ν(N≡N) initiation. The same transport speeds of 8.0 ± 0.3 Å/ps and 8.0 ± 0.2 Å/ps were found for CH*n*-a and CH*n*-s initiated by ν(C═O) and ν_{as}(C═O), respectively (Figure 6D, filled symbols). Such fast transport speeds via alkane chains suggest ballistic nature of the transport.

5. ADDITIVITY OF THE TRANSPORT

Several general stages can be considered for the energy transport in oligomers in these experiments: (I) vibrational relaxation of the tag, arrival of excess energy to the beginning of the chain, and formation of the wavepacket (wavepacket initiation), (II) energy transport through the chain (wavepacket motion), (III) wavepacket relaxation to another end group, and, if needed, transport within the end group to the reporter site (excess energy detection) (Figure 7A). Similar transport stages occur in SAM junctions (Figure 7B). Each stage requires a certain amount of time, thus affecting the overall energy transport time. For example, the diffusive transport to the chain from the ν_{as}(C═O) tag takes over 3 ps (Figure 6D). To test if the ballistic transport steps are additive with the diffusive steps of the process, experiments were performed with the CH*n*-s

DOI: 10.1021/acs.accounts.5b00299
Acc. Chem. Res. 2015, 48, 2547–2555

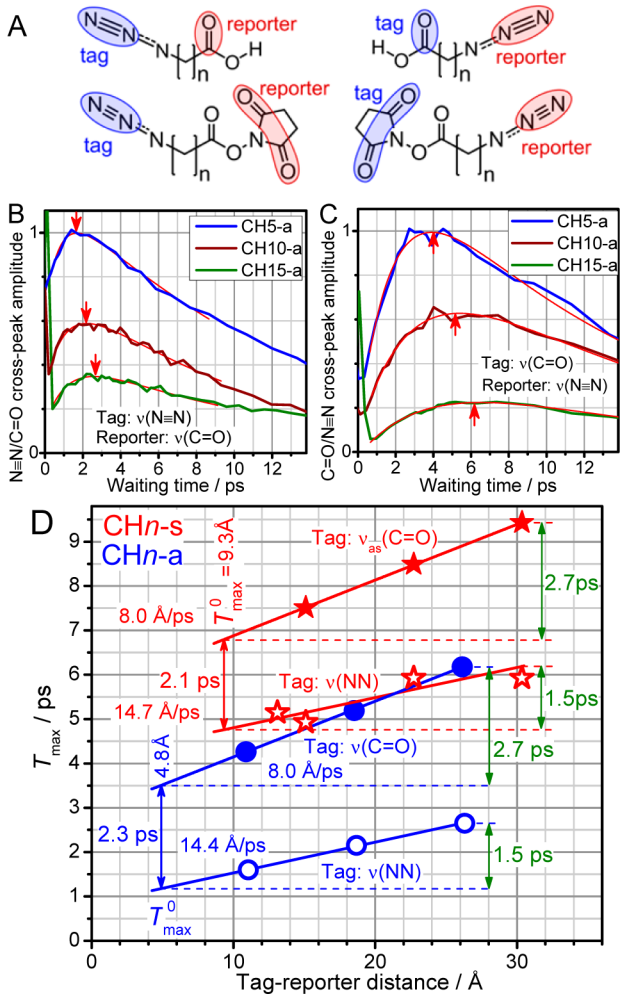

Figure 6. Ballistic energy transport via alkane chains. (A) Combinations of tags and reporters interrogated via RA 2DIR. (B and C) Waiting time dependences for the indicated cross peaks for CH*n*-a. The fit with a two-exponential function is shown (red), and the T_{max} values obtained from the fit are indicated by arrows. (D) T_{max} values plotted as a function of the tag-reporter distance for the transport initiated in CH*n*-a and CH*n*-s by ν(C═O), ν_{as}(C═O), and ν(N≡N) modes. The linear fits are shown with lines; the zero-chain-length distances of 4.8 and 9.3 Å are indicated for CH*n*-a and CH*n*-s, respectively.

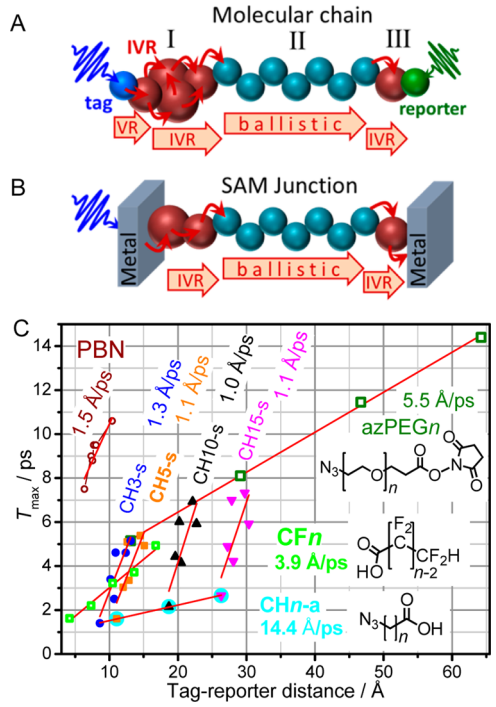

Figure 7. Characteristic stages of energy transport in oligomers (A) and SAM junctions (B). (C) Cumulative graph showing the data obtained for different series of compounds (indicated).

compounds using the ν(N≡N) tag and different reporters at the succinimide ester group. Figure 7C summarizes the results for CH3-s (blue), CH5-s (orange), CH10-s (black), and CH15-s (magenta); the linear fits (lines) resulted in similar speeds for all of the compounds indicating additivity of the diffusive and ballistic times. Interestingly, the effective speed of diffusive transport is found at 1.0−1.3 Å/ps, corresponding approximately to passing one bond length per one picosecond, which is a lifetime of a typical vibrational mode in large organic molecules. Such interpretation permits estimating the diffusive transport time by the number of bonds to be traveled − 1 ps per bond. For example, for the transport initiated in CH15-s by ν(N≡N), there is one VR step at the azido group (ν(N≡N) lifetime of 1.1 ps) and ∼3 bonds to reach the succinimide site, one picosecond each, amounting to 4.1 ps. The through-chain transport is ballistic with a speed of 14.7 Å/ps, amounting to 1.7 ps. The overall transport time, 4.1 + 1.7 = 5.8 ps, matches the experimental T_{max} value of 5.9 ps. The transport time for CH10-a initiated by ν(N≡N) is composed of the relaxation step at the azido group (1.1 ps) and ballistic transport via the chain (1.15 ps); the reporter ν(C═O) is attached to the chain and may not require additional diffusive steps. Indeed, the calculated time, 2.25 ps, matches well with the experimental value of 2.15 ps. The observed additivity suggests that the same quantum of energy is delivered to the end group regardless of the chain length, thus confirming the ballistic nature of the transport in the chain.

Although the transport via alkane chains is fast, the T_{max} values measured for the ν_{as}(C═O) initiation and ν(N≡N) detection are alarmingly large for a ballistic transport, exceeding 9 ps (Figure 6D). Note that ballistic transport is a coherent process requiring that the wavepacket preserves its coherence for the time of the transport and does not undergo scattering. Consideration of all transport stages helps in understanding the overall process. One can evaluate the T_{max} values (T^0_{max}) corresponding to the zero-chain-length tag-reporter distances taken at 4.8 and 9.3 Å for CH*n*-a and CH*n*-s, respectively (Figure 6D). For the transport initiated in CH*n*-a by the ν(N≡N) tag, the T^0_{max} value is ∼1.2 ps, which is close to the ν(N≡N) lifetime (1.1 ps). For the transport initiated by ν(C═O), the T^0_{max} value (∼3.5 ps) is much larger than the ν(C═O) lifetime of 1.2 ps.[35] It is conceivable that the difference describes additional diffusive IVR steps required to reach the reporter (ν(N≡N)) site from the chain, whereas relaxation of the ν(N≡N) tag directly generates the wavepacket in the chain. If so, a similar difference in T^0_{max} values is expected for the transports initiated by ν(N≡N) and ν_{as}(C═O) in CH*n*-s, which is indeed so (2.1 ps, Figure 6D). This observation shows that the diffusive steps themselves are not additive and that the transport time depends on the frequency range of the modes involved. The longest ballistic transport times (measured in CH15) are shown in Figure 6D with green numbers, equaling

DOI: 10.1021/acs.accounts.5b00299
Acc. Chem. Res. 2015, 48, 2547−2555

1.5 and 2.7 ps for the transport initiated by ν(N≡N) and ν(C═O), respectively. Importantly, large T_{max} for CH15-s with ν_{as}(C═O) initiation (9.4 ps) is split between the tag lifetime (1.1 ps), diffusive steps at the tag site to reach the chain (~3.5 ps, given by the separation between the parallel red and blue lines in Figure 6E), ballistic transport time (~2.7 ps), and diffusive steps at the reporter site (2.1−2.3 ps).

6. ANALYSIS OF THE CHAIN BANDS

Different ballistic transport speeds found for different chains and for different cases of transport initiation within the same chain type clearly suggest that different chain bands are participating in the transport for different cases. Each chain band has a characteristic group velocity for transporting a wavepacket. For these velocities to be found, the chain band structure (dispersion relations) was calculated for alkanes.[41,42] The Hessian matrix of force constants for the alkane chain was obtained from the DFT normal-mode analysis for CH15-a, adopting the all-anti conformation. The nearest and next-nearest cell interactions were included in the Hamiltonian (Figure 8A).[42] Ten lowest-energy optical bands for alkane chains are shown in Figure 8B. Bands of the same motion type are plotted with the same color. Each thick line comprises two optical bands, one band in the wavevector (q) region from 0 to π/a and the other from π/a to $2\pi/a$, where a is the unit-cell length. Because of translational invariance of the unit cell selection by half the cell, the two bands of the same type have the same energies and derivatives at $q = \pi/a$; each pair is referred to by the motion type (e.g., CH_2 rocking, CC stretching, etc). For chains with a finite length, the number of states in each band pair equals the number of CH_2 groups in the chain; the chain states are evenly spaced along the abscissa in Figure 8B.[42]

If a superposition state involving a specific chain band is formed in the chain as a spatially bell-shaped wavepacket, it will propagate with time along the chain with the group velocity dictated by the involved states. The group velocity for a narrow range of frequencies centered at $\omega_0(q_0)$ is determined as $V(q_0) = (\partial\omega/\partial q)|_{q=q_0}$. Because the group velocity (slope in Figure 8B) is different for different ranges of frequencies involved, the mean group velocity over a selected range of wavevectors from q_1 to q_2 is computed as $\langle V\rangle = (q_2 - q_1)^{-1}\int_{q_1}^{q_2}|V(q)|\,dq$. The mean group velocities corresponding to the whole bands are given in Figure 8B on the right; the values vary greatly from band to band. The dominating IVR pathways originated from the excited tag determine the chain band(s) that will participate the most in the through-chain transport.[42]

7. END-GROUP RELAXATION PATHWAYS LEAD TO WAVEPACKET FORMATION

The small value of T^0_{max} for the transport initiated in CHn-a by ν(N≡N) (~1.2 ps, Figure 6D) suggests that the wavepacket in the chain is formed directly from relaxation of the nu(CN) mode. The analysis of the relaxation (IVR) channels[31,32] of ν(N≡N) showed the dominance of a single relaxation channel: ν(N≡N) → ν(N═N) + ν(N−C) (Figure 8C).[42] It is expected that at least one of these modes is strongly coupled to the chain states. The ν(N═N) mode frequency falls within two chain bands, corresponding to the CH_2 wagging and twisting motions (Figure 8B), whereas the ν(N−C) mode frequency matches the CH_2 rocking band of the chain. The width of the ν(N−C) transition is small, ~12 cm^{-1}, resulting in a few or no resonances with the chain states (CH_2 rocking) and poor quality of a possible wavepacket.

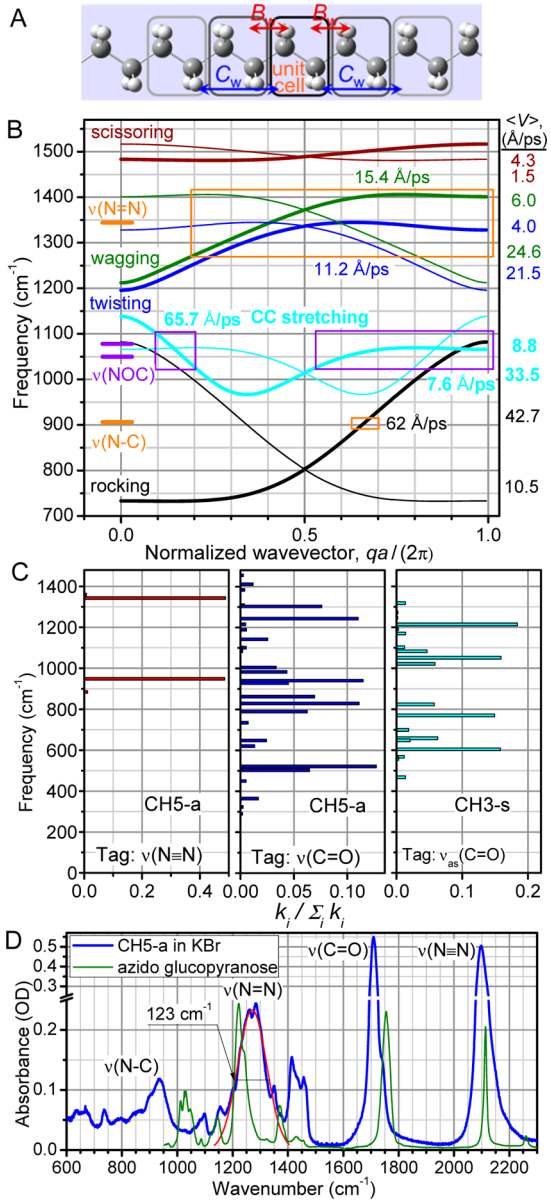

Figure 8. Computed optical bands of alkane chains and tag relaxation pathways. (A) Alkane unit cell and the interactions of the central cell included in the calculations. (B) Ten lowest-energy optical bands for the alkane chain as a function of a normalized wavevector. The boxes match the width of the azido-group stretching modes, ν(N═N) and ν(C−N) (orange) and ν(NOC) (violet). (C) Rates of all relaxation channels of the ν(N≡N), ν(C═O), and ν_{as}(C═O) tags in the indicated compounds, normalized in each case by the sum of all respective rate constants ($k_i/\sum_i k_i$), where k_i is the rate of an individual third-order IVR pathway.[31,32] (D) Linear absorption spectra for CH5-a in a KBr pellet (blue) and 1,3,4,6-tetra-*O*-acetyl-2-azido-2-deoxy-α-D-glucopyranose (green) in $CDCl_3$ are shown for comparison.

Importantly, the ν(N═N) transition is very broad with the full width at half-maximum (fwhm) of 123 cm^{-1} (Figure 8D). There are many chain states within its bandwidth that offer relaxation channels (Figure 8B, box). An assumption that the lifetime broadening dominates the width leads to the ν(N═N) lifetime of 44 fs.[42] The widths of the wavepackets formed in the CH_2 wagging and twisting chain bands were taken as the width

DOI: 10.1021/acs.accounts.5b00299
Acc. Chem. Res. 2015, 48, 2547−2555

of the ν(N═N) transition, which resulted in the group velocities of 15.4 and 11.2 Å/ps, respectively. The coupling of ν(N═N) to CH_2 wagging and twisting chain states depends on the conformation at the azido group attachment to the chain: the anti conformation favors relaxation into the wagging states, whereas gauche permits relaxation into both bands.[42] As the energy difference for the two conformers is small, no clear preference for the involvement of the two bands was made. The velocities supported by both bands are close to the experimental value of 14.4 Å/ps, so both bands, CH_2 wagging and twisting, are believed to contribute significantly to the transport initiated by ν(N≡N).

For the transport initiated by ν(C═O) in CH*n*-a and ν_{as}(C═O) in CH*n*-s, numerous relaxation channels are found (Figure 8C). In CH*n*-s, the ν_{as}(C═O) tag is located 3 bonds away from the chain, requiring several IVR steps for the energy to reach the chain. Note that the acoustic bands are coupled strongly to the solvent and are unlikely to transfer energy efficiently within the molecule.[17] The stretching modes of the ester, ν_{as}(NOC) at 1083 cm^{-1} and ν_{ss}(NOC) at 1052 cm^{-1}, being the only high-frequency ester modes accessible from the ν_{as}(C═O) relaxation, were suggested to be doorway modes capable of transferring energy into the optical bands of the chain (Figure 8A). Their frequencies match several band branches (two CC stretching and one CH_2 rocking), but only the CC stretching bears large density of states and a speed (7.6 Å/ps, Figure 8B, violet box) that matches the experimental speed (8.0 Å/ps). Analysis of the coupling of the doorway states to the CC stretching relative to CH_2 rocking modes, performed for the Boltzmann weighted conformation distribution at the chain-ester connection (Figure 9A), showed that the former is ~13-fold larger than the latter (Figure 9B,C). Thus, it was concluded that the CC stretching chain band is responsible for the transport initiated by ν_{as}(C═O). On the basis of the similarity of the speeds obtained for the transport in CH*n*-a and CH*n*-s, the CC stretching chain band was suggested as the main energy transporter for both cases.

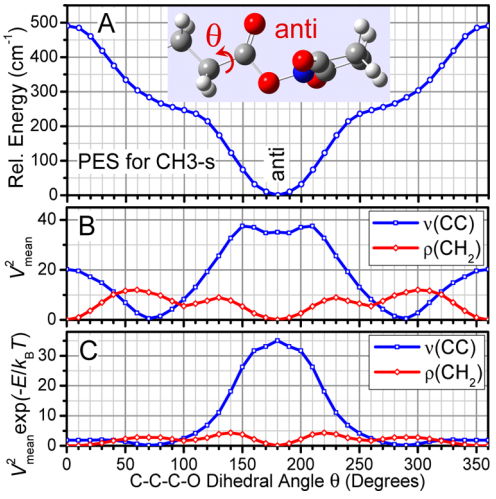

Figure 9. Coupling-based selection of the dominant chain band transporter. (A) DFT-computed potential energy surface for CH3-s along the C-C-C-O dihedral angle (θ). Mean-square coupling strength of ν(NOC) with the CC stretching and CH_2 rocking states (B) and their values weighted by the Boltzmann factor (C). The ratio of the integrals under the curves in panel (C) equals 4.4; multiplication by the density of states ratio (~3) results in ~13-fold dominance of the relaxation into CC stretching vs the CH_2 rocking band.

8. DIFFERENT WAYS OF WAVEPACKET INITIATION

Efficient energy transport to large distances requires the formation of a spatially confined wavepacket; such a wavepacket needs a large number of chain states to participate in the superposition. For a large group velocity, the states for the wavepacket should cover a substantial range of frequencies. Designing relaxation processes capable of exciting a broad range of frequencies of the targeted chain band is essential for having efficient through-chain energy transport. Vibrational relaxation of ν(N≡N) at the azido moiety provides such an opportunity with a group velocity of 14.4 Å/ps. However, much higher group velocities can be supported by other alkane bands (Figure 8B). Alternatively, the ν(N═N) mode of the azido moiety can be excited directly with the mid-IR pulses (Figure 10). The spectral width of the mid-IR pulses, fwhm ~ 170 cm^{-1}, is sufficient for efficiently exciting the ν(N═N) mode; thus, a similar energy transport speed to that initiated by ν(N≡N) is expected. Indeed, the transport speed is found to be 11 ± 4 Å/ps (Figure 10), although the error bars are large, caused by other transitions excited at the same time at the succinimide ester moiety.[42] The T^0_{max} value, 3.8 ps, is ~0.9 ps shorter than that for the transport initiated by ν(N≡N) (Figure 6D), suggesting that the overall transport time became shorter approximately by the ν(N≡N) lifetime (1.1 ps), confirming that the chain wavepacket was generated directly by the mid-IR pulses. Note that a localized N═N stretching motion is responsible for the IR intensity of the peak at 1270 cm^{-1}, as the chain states of alkanes are essentially dark.

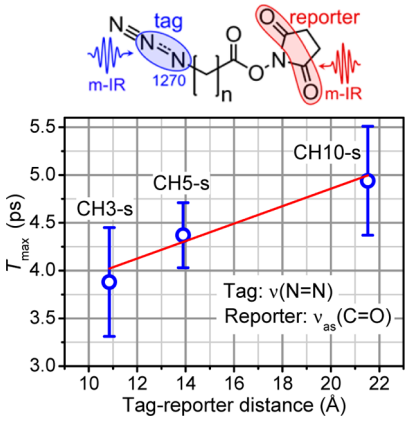

Figure 10. Dependence of T_{max} on tag-reporter distance obtained for the energy transport initiated by the ν(N═N) tag in CH*n*-s. The linear fit (red) resulted in the transport speed of 11 ± 4 Å/ps.

■ CONCLUDING REMARKS

The studies overviewed in this Account show that the speed of the energy transport process in oligomers can be designed to meet specific requirements. The overall transport time is governed by the intrinsic chain properties as well as by transport initiation. Although chains with stiffer backbones are generally capable of transporting energy faster, the match of the end group states with the states of the chain could be more important.[43] Note that in the thermal conductivity measurements performed at quasi-equilibrium conditions, the ballistic transport results in the temperature gradients only at the

DOI: 10.1021/acs.accounts.5b00299
Acc. Chem. Res. 2015, 48, 2547−2555

contacts; thus, the chain transport properties are difficult to study.[14,17,44] The time-resolved RA 2DIR experiments permit resolving each transport stage separately, and different transport speeds through the chain are found depending on the end group involved (contacts). Certainly, the through-chain transport takes a significant amount of time in oligomers: for example, for the transport initiated in CH15-a by ν(N≡N), the overall transport time ($T_{max} \sim 2.7$ ps) is split between the wavepacket initiation (1.2 ps) and the through-chain ballistic transport (1.5 ps). Interestingly, in perfluoroalkanes, the wavepacket coherence time of 3.3 ps is required for fully ballistic transport in CF11; the temperature dependences indicate transitions to diffusive transport at higher temperatures in these chains.[40,45] The mean free path for a variety of chain types was found to be 12−15 Å.[35,36,40] Further efforts may aim to attain larger propagation speeds and greater transport efficiencies, exploiting the chain bands featuring high group velocities and slow dephasing. It is also important to understand wavepacket scattering and relaxation processes and how they depend on the intersite couplings. Understanding the role different system parameters, such as chain architecture and temperature, play in energy transport can help in designing molecular systems for molecular electronics with targeted heat management properties.

■ ASSOCIATED CONTENT

Supporting Information

The Supporting Information is available free of charge on the ACS Publications website at DOI: 10.1021/acs.accounts.5b00299.

T_{max} transport speeds and mean free paths for various classes of compounds along with computational details (PDF)

■ AUTHOR INFORMATION

Corresponding Author

*E-mail: irubtsov@tulane.edu.

Notes

The authors declare no competing financial interest.

Biographies

Natalia Rubtsova received an M.S. in Chemistry from Lomonosov Moscow State University in 2008. Currently, she is a Ph.D. candidate at Tulane University studying ballistic energy transport in molecules under the supervision of Prof. Rubtsov.

Layla Qasim obtained a B.S. in Chemistry and minor in Mathematics from Northern Arizona University. She is currently working towards a Ph.D. studying ballistic vibrational energy transport in polymers under the supervision of Prof. Rubtsov.

Arkady Kurnosov obtained an M.S. in Physics from Lomonosov Moscow State University. Currently, he is a Ph.D. candidate working on the theory of vibrational energy transport in molecules under the supervision of Prof. Burin.

Alexander Burin graduated from Moscow Institute for Engineering and Physics and received his Ph.D. from the same institute (1989). He has been a faculty member at Tulane University since 2003. His current research interests include the investigation of complex dynamics of many-body systems, including nonlinear molecular vibrations.

Igor Rubtsov received his M.S. degree from Moscow Institute for Physics and Technology and Ph.D. from the Institute for Chemical Physics in Moscow. He is currently a Professor of Chemistry at Tulane University. His research interests include energy and charge transport processes and the development of multidimensional spectroscopy methods.

■ ACKNOWLEDGMENTS

This work was supported by the National Science Foundation (CHE-1462075) and Tulane Bridge Fund. Construction of the fully automated 2DIR instrument was supported by the National Science Foundation MRI grant (CHE-1040491) and by the Louisiana Board of Regents (LEQSF(2011-12)-ENH-TR-29).

■ REFERENCES

(1) Chang, C. W.; Okawa, D.; Majumdar, A.; Zettl, A. Solid-state thermal rectifier. *Science* **2006**, *314*, 1121−1124.
(2) Yu, C.; Shi, L.; Yao, Z.; Li, D.; Majumdar, A. Thermal Conductance and Thermopower of an Individual Single-Wall Carbon Nanotube. *Nano Lett.* **2005**, *5*, 1842−1846.
(3) Pernot, G.; Stoffel, M.; Savic, I.; Pezzoli, F.; Chen, P.; Savelli, G.; Jacquot, A.; Schumann, J.; Denker, U.; Monch, I.; Deneke, C.; Schmidt, O. G.; Rampnoux, J. M.; Wang, S.; Plissonnier, M.; Rastelli, A.; Dilhaire, S.; Mingo, N. Precise control of thermal conductivity at the nanoscale through individual phonon-scattering barriers. *Nat. Mater.* **2010**, *9*, 491−495.
(4) Majumdar, S.; Sierra-Suarez, J. A.; Schiffres, S. N.; Ong, W.-L.; Higgs, C. F.; McGaughey, A. J. H.; Malen, J. A. Vibrational Mismatch of Metal Leads Controls Thermal Conductance of Self-Assembled Monolayer Junctions. *Nano Lett.* **2015**, *15*, 2985−2991.
(5) Nitzan, A.; Ratner, M. A. Electron Transport in Molecular Wire Junctions. *Science* **2003**, *300*, 1384−1389.
(6) Losego, M. D.; Grady, M. E.; Sottos, N. R.; Cahill, D. G.; Braun, P. V. Effects of chemical bonding on heat transport across interfaces. *Nat. Mater.* **2012**, *11*, 502−506.
(7) Tian, Z.; Marconnet, A.; Chen, G. Enhancing solid-liquid interface thermal transport using self-assembled monolayers. *Appl. Phys. Lett.* **2015**, *106*, 211602(1−4).
(8) Shen, S.; Henry, A.; Tong, J.; Zheng, R.; Chen, G. Polyethylene nanofibres with very high thermal conductivities. *Nat. Nanotechnol.* **2010**, *5*, 251−255.
(9) Henry, A.; Chen, G. High thermal conductivity of single polyethylene chains using molecular dynamics simulations. *Phys. Rev. Lett.* **2008**, *101*, 235502(1−4).
(10) Nitzan, A. Molecules take the heat. *Science* **2007**, *317*, 759−760.
(11) Carter, J. A.; Wang, Z.; Dlott, D. D. Ultrafast nonlinear coherent vibrational sum-frequency spectroscopy methods to study thermal conductance of molecules at interfaces. *Acc. Chem. Res.* **2009**, *42*, 1343−1351.
(12) Wang, Z.; Carter, J. A.; Lagutchev, A.; Koh, Y. K.; Seong, N.-H.; Cahill, D. G.; Dlott, D. D. Ultrafast flash thermal conductance of molecular chains. *Science* **2007**, *317*, 787−790.
(13) Meier, T.; Menges, F.; Nirmalraj, P.; Hölscher, H.; Riel, H.; Gotsmann, B. Length-Dependent Thermal Transport along Molecular Chains. *Phys. Rev. Lett.* **2014**, *113*, 060801(1−6).
(14) Cahill, D. G.; Ford, W. K.; Goodson, K. E.; Mahan, G. D.; Majumdar, A.; Maris, H. J.; Merlin, R.; S.R, P. Nanoscale thermal transport. *J. Appl. Phys.* **2003**, *93*, 793−818.
(15) Minnich, A. J.; Johnson, J. A.; Schmidt, A. J.; Esfarjani, K.; Dresselhaus, M. S.; Nelson, K. A.; Chen, G. Thermal conductivity spectroscopy technique to measure phonon mean free paths. *Phys. Rev. Lett.* **2011**, *107*, 095901(1−4).
(16) Siemens, M. E.; Li, Q.; Yang, R.; Nelson, K. A.; Anderson, E. H.; Murnane, M. M.; Kapteyn, H. C. Quasi-ballistic thermal transport from nanoscale interfaces observed using ultrafast coherent soft X-ray beams. *Nat. Mater.* **2010**, *9*, 26−30.

DOI: 10.1021/acs.accounts.5b00299
Acc. Chem. Res. 2015, 48, 2547−2555

(17) Segal, D.; Nitzan, A.; Hanggi, P. Thermal conductance through molecular wires. *J. Chem. Phys.* **2003**, *119*, 6840−6855.
(18) Schwarzer, D.; Kutne, P.; Schroeder, C.; Troe, J. Intramolecular vibrational energy redistribution in bridged azulene-anthracene compounds: Ballistic energy transport through molecular chains. *J. Chem. Phys.* **2004**, *121*, 1754−1764.
(19) Backus, E. H. G.; Bloem, R.; Pfister, R.; Moretto, A.; Crisma, M.; Toniolo, C.; Hamm, P. Dynamical Transition in a Small Helical Peptide and Its Implication for Vibrational Energy Transport. *J. Phys. Chem. B* **2009**, *113*, 13405−13409.
(20) Kurochkin, D. V.; Naraharisetty, S. G.; Rubtsov, I. V. Relaxation-assisted 2DIR spectroscopy method. *Proc. Natl. Acad. Sci. U. S. A.* **2007**, *104*, 14209−14214.
(21) Rubtsov, I. V. Relaxation-assisted 2DIR: Accessing distances over 10Å and measuring bond connectivity patterns. *Acc. Chem. Res.* **2009**, *42*, 1385−1394.
(22) Naraharisetty, S. G.; Kasyanenko, V. M.; Rubtsov, I. V. Bond connectivity measured via relaxation-assisted two-dimensional infrared spectroscopy. *J. Chem. Phys.* **2008**, *128*, 104502/1−104502/7.
(23) Rubtsova, N. I.; Rubtsov, I. V. Vibrational Energy Transport in Molecules Studied by Relaxation-Assisted Two-Dimensional Infrared Spectroscopy. *Annu. Rev. Phys. Chem.* **2015**, *66*, 717−738.
(24) Hamm, P.; Lim, M.; Hochstrasser, R. M. Structure of the amide I band of peptides measured by femtosecond non-linear infrared spectroscopy. *J. Phys. Chem. B* **1998**, *102*, 6123−6138.
(25) Asplund, M. C.; Zanni, M. T.; Hochstrasser, R. M. Two-dimensional infrared spectroscopy of peptides by phase-controlled femtosecond vibrational photon echoes. *Proc. Natl. Acad. Sci. U. S. A.* **2000**, *97*, 8219−8224.
(26) Lin, Z.; Keiffer, P.; Rubtsov, I. V. A method for determining small anharmonicity values from 2DIR spectra using thermally induced shifts of frequencies of high-frequency modes. *J. Phys. Chem. B* **2011**, *115*, 5347−5353.
(27) Rubtsov, I. V.; Wang, J.; Hochstrasser, R. M. Dual frequency 2D-IR heterodyned photon-echo of the peptide bond. *Proc. Natl. Acad. Sci. U. S. A.* **2003**, *100*, 5601−5606.
(28) Leger, J.; Nyby, C.; Varner, C.; Tang, J.; Rubtsova, N. I.; Yue, Y.; Kireev, V.; Burtsev, V.; Qasim, L.; Rubtsov, G. I.; Rubtsov, I. V. Fully automated dual-frequency three-pulse-echo 2DIR spectrometer accessing spectral range from 800 to 4000 wavenumbers. *Rev. Sci. Instrum.* **2014**, *85*, 083109(1−16).
(29) Mueller-Werkmeister; M, H.; Li, Y.-L.; Lerch, E.-B. W.; Bigourd, D.; Bredenbeck, J. Ultrafast Hopping from Band to Band: Assigning Infrared Spectra based on Vibrational Energy Transfer. *Angew. Chem., Int. Ed.* **2013**, *52*, 6214−6217.
(30) Kasyanenko, V. M.; Tesar, S. L.; Rubtsov, G. I.; Burin, A. L.; Rubtsov, I. V. Structure dependent energy transport: Relaxation-assisted 2DIR and theoretical studies. *J. Phys. Chem. B* **2011**, *115*, 11063−11073.
(31) Tesar, S. L.; Kasyanenko, V. M.; Rubtsov, I. V.; Rubtsov, G. I.; Burin, A. L. Theoretical study of internal vibrational relaxation and energy transport in polyatomic molecules. *J. Phys. Chem. A* **2013**, *117*, 315−323.
(32) Burin, A. L.; Tesar, S. L.; Kasyanenko, V. M.; Rubtsov, I. V.; Rubtsov, G. I. Semiclassical model for vibrational dynamics of polyatomic molecules: Investigation of Internal Vibrational Relaxation. *J. Phys. Chem. C* **2010**, *114*, 20510−20517.
(33) Kuzmin, M.; Stuchebrukhov, A. A. In *Laser spectroscopy of highly vibrationally excited molecules*; Letokhov, V. S., Ed.; Hilger: New York, 1989.
(34) Logan, D. E.; Wolynes, P. G. Quantum localization and energy flow in many-dimensional Fermi resonant systems. *J. Chem. Phys.* **1990**, *93*, 4994(1−19).
(35) Rubtsova, N. I.; Nyby, C. M.; Zhang, H.; Zhang, B.; Zhou, X.; Jayawickramarajah, J.; Burin, A. L.; Rubtsov, I. V. Room-temperature ballistic energy transport in molecules with repeating units. *J. Chem. Phys.* **2015**, *142*, 212412(1−8).
(36) Lin, Z.; Zhang, N.; Jayawickramarajah, J.; Rubtsov, I. V. Ballistic energy transport along PEG chains: Distance dependence of the transport efficiency. *Phys. Chem. Chem. Phys.* **2012**, *14*, 10445−10454.
(37) Lin, Z.; Rubtsov, I. V. Constant-speed vibrational signaling along polyethyleneglycol chain up to 60-Å distance. *Proc. Natl. Acad. Sci. U. S. A.* **2012**, *109*, 1413−1418.
(38) Teraoka, I. *Polymer solutions*; Wiley & Sons, Inc.: New York, 2002.
(39) Rubtsova, N. I.; Rubtsov, I. V. Ballistic energy transport via perfluoroalkane linkers. *Chem. Phys.* **2013**, *422*, 16−21.
(40) Rubtsova, N. I.; Kurnosov, A. A.; Burin, A. L.; Rubtsov, I. V. Temperature dependence of the ballistic energy transport in perfluoroalkanes. *J. Phys. Chem. B* **2014**, *118*, 8381−8387.
(41) Tasumi, M.; Shimanouchi, T.; Miyazawa, T. Normal Vibrations and Force Constants of Polymethylene Chain. *J. Mol. Spectrosc.* **1962**, *9*, 261−287.
(42) Yue, Y.; Qasim, L. N.; Kurnosov, A. A.; Rubtsova, N. I.; Mackin, R. T.; Zhang, H.; Zhang, B.; Zhou, X.; Jayawickramarajah, J.; Burin, A. L.; Rubtsov, I. V. Band-Selective Ballistic Energy Transport in Alkane Oligomers: Towards Controlling the Transport Speed. *J. Phys. Chem. B* **2015**, *119*, 6448−6456.
(43) Leitner, D. M. Thermal Boundary Conductance and Thermal Rectification in Molecules. *J. Phys. Chem. B* **2013**, *117*, 12820−12828.
(44) Schmidt, M.; Kottos, T.; Shapiro, B. Random-matrix-theory approach to mesoscopic fluctuations of heat current. *Phys. Rev. E* **2013**, *88*, 022126(1−5).
(45) Kurnosov, A. A.; Rubtsov, I. V.; Burin, A. L. Fast transport and relaxation of vibrational energy in polymer chains. *J. Chem. Phys.* **2015**, *142*, 011101/1−011101/4.

DOI: 10.1021/acs.accounts.5b00299
Acc. Chem. Res. 2015, 48, 2547−2555